Instability of a shallow-water potential-vorticity front

By DAVID G. DRITSCHEL[1]
AND JACQUES VANNESTE[2]

[1]School of Mathematics and Statistics, University of St Andrews, St Andrews KY16 9SS, UK
e-mail: dgd@mcs.st-and.ac.uk

[2]School of Mathematics, University of Edinburgh, King's Buildings, Edinburgh EH9 3JZ, UK
e-mail: j.vanneste@ed.ac.uk

A straight front separating two semi-infinite regions of uniform potential vorticity (PV) in a rotating shallow-water fluid gives rise to a localised fluid jet and a geostrophically-balanced shelf in the free surface. The linear stability of this configuration, consisting of the simplest non-trivial PV distribution, has been studied previously, with ambiguous results. We revisit the problem and show that the flow is weakly unstable when the maximum Rossby number $R > 1$. The instability is surprisingly weak, indeed exponentially so, scaling like $\exp[-4.3/(R-1)]$ as $R \to 1$. Even when $R = \sqrt{2}$ (when the maximum Froude number $F = 1$), the maximum growth rate is only 7.76×10^{-6} times the Coriolis frequency. Its existence nonetheless sheds light on the concept of 'balance' in geophysical flows, i.e. the degree to which the PV controls the dynamical evolution of these flows.

1. Introduction

Two nearly distinct types of motion are found in the Earth's atmosphere and oceans, namely 'balanced' vortical motions and 'unbalanced' gravity-wave motions. The balanced motions are controlled entirely by a materially advected scalar, the potential vorticity (PV), from which all other dynamical fields (velocity, pressure, etc.) can be derived via *prescribed* 'inversion relations'. The residual motions are classified as unbalanced motions, and are presumed to be gravity waves.

This decomposition is only strictly defined however for the linearised equations about a state of rest. Otherwise, a degree of ambiguity arises (surrounding the choice of inversion relations, for instance), making it impossible to uniquely define the balanced part of the flow (cf. Mohebalhojeh & Dritschel 2001, Viúdez & Dritschel 2004 and references therein). Nevertheless, such a decomposition, even if inexact, is often of great practical utility, particularly in weather forecasting. The actual ambiguity in the definition of balance can be exceedingly small in many circumstances.

A long-standing problem in geophysical fluid dynamics concerns the quantification of the coupling between the two types of motion and, in particular, the mechanisms for the generation of gravity waves by balanced motion (e.g. Lorenz & Krishnamurthy 1987, Warn 1997, Ford, McIntyre & Norton 2000, Vanneste 2004 and references therein). Among these mechanisms, unbalanced instabilities of steady (balanced) flows have recently received a great deal of attention (e.g., Ford 1994, Yavneh, Molemaker & McWilliams 2001, McWilliams, Molemaker & Yavneh 2004, Plougonven, Muraki & Snyder 2005). These instabilities have several significant features: with their growing modes of mixed
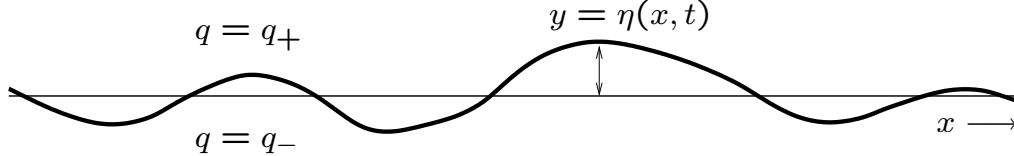
FIGURE 1. Schematic diagram of a disturbed PV front. In the linear stability analysis, the displacement η is taken to be purely sinusoidal.

nature, they reveal, in a simple context, the coupling that exists between balanced and unbalanced motion in a basic state flow *not* at rest, and it has been suggested that they may contribute to energy dissipation of balanced flows (McWilliams, Molemaker & Yavneh 2001).

Here, we focus, or rather refocus, on the simplest instability mechanism of this type. We consider a shallow-water flow, rotating uniformly at rate $f/2$, on an infinite plane, and choose the simplest non-trivial PV distribution, namely that of a single step discontinuity along a front $y = \eta(x, t)$, whose undisturbed position is $y = 0$ (see figure 1). This configuration admits a single balanced or vortical wave, known as a Rossby wave, which predominantly displaces the interface. It also admits an infinite set of gravity waves, just as in the case of a basic state at rest. We furthermore consider only the *linear* dynamics, specifically the linear stability of this configuration. This was first done, for a special case, by Paldor (1983), then in the general case studied here by Boss, Paldor & Thompson (1996). Those studies concluded that the front is linearly stable for all parameters (here the Froude or Rossby number characterising the basic flow, and the x wavenumber of the disturbance k).

A re-examination, however, indicates that instability occurs whenever the maximum Rossby number R exceeds unity. This occurs when the maximum Froude number F (measuring the maximum flow speed to local gravity wave speed) exceeds $1/\sqrt{2}$. Indeed, the existence of this instability was first demonstrated in the PhD thesis of Ford (1993), but was dismissed by Boss *et al.*(1996) on the grounds that the disturbance mode had unbounded energy. This is not the case. The mode decays exponentially far from the front, and hence has finite energy. Note that for $\mathsf{R} < 1$, i.e. $\mathsf{F} < 1/\sqrt{2}$, formal stability can be established by Ripa's (1983) theorem (Ford 1993).

The observed growth rates, some 5-6 orders of magnitude smaller than f, require highly-accurate numerics to capture. Here, we extend the work of Ford (1993) by examining the parameter space more comprehensively, especially the regime $\mathsf{F} \leqslant 1$. This is done both numerically and analytically, using a WKB analysis that provides estimates for the instability growth rate as $\mathsf{R} \to 1$. The analysis presented here enables an accurate estimate of the threshold and maximum wavenumbers for instability, as well as a good estimate of the growth rates.

The observed instability points to a breakdown of the concept of balance *in a linear system* when $\mathsf{R} > 1$. This is probably the simplest fluid-dynamical context in which this occurs. The extremely small growth rates indicate that balance may dominate even in parameter regimes where there is no frequency separation between balanced and unbalanced motions. This finding provides theoretical support to the observation that rotating flows are often close to some form of balance even in the absence of a frequency separation.

The structure of the paper is as follows. The next section presents the governing equations, the basic state, the linear system to be analysed, and the solution procedure. This is followed in §§3 and 4 by numerical results and the asymptotic analysis, including comparisons and careful checks on accuracy. The paper concludes in §5 with some implications and a discussion of the nonlinear problem.

2. Formulation

2.1. *Mathematical model*

We consider an unbounded inviscid rotating shallow fluid layer held down by gravity. Its evolution is modelled by the shallow-water equations

$$\frac{\partial u}{\partial t} + u\frac{\partial u}{\partial x} + v\frac{\partial u}{\partial y} - fv = -\frac{\partial \phi}{\partial x} \tag{2.1}$$

$$\frac{\partial v}{\partial t} + u\frac{\partial v}{\partial x} + v\frac{\partial v}{\partial y} + fu = -\frac{\partial \phi}{\partial y} \tag{2.2}$$

$$\frac{\partial \phi}{\partial t} + \frac{\partial (u\phi)}{\partial x} + \frac{\partial (v\phi)}{\partial y} = 0 \tag{2.3}$$

where f is the Coriolis parameter (twice the background rotation rate), u and v are the x and y velocity components, and $\phi = gh$ is the geopotential (cf. Gill 1982). Note that these equations exploit the hydrostatic approximation, strictly valid only when $h/L \ll 1$, where L is a characteristic horizontal scale.

The above equations can be combined to prove that the potential vorticity

$$q = \frac{\partial v/\partial x - \partial u/\partial y + f}{\phi} \tag{2.4}$$

is *materially conserved* following fluid particles, i.e.

$$\frac{\mathrm{D}q}{\mathrm{D}t} = \frac{\partial q}{\partial t} + u\frac{\partial q}{\partial x} + v\frac{\partial q}{\partial y} = 0.$$

Hence, contours of constant q move with the fluid.

The simplest non-trivial PV distribution imaginable consists of a single PV *jump* or front separating two regions of uniform q in the plane. Let $y = \eta(x,t)$ denote the position of the front at time t (in the linear analysis below, $\partial\eta/\partial x \ll 1$). Then conservation of q reduces to

$$\frac{\partial \eta}{\partial t} + u(x,\eta,t)\frac{\partial \eta}{\partial x} = v(x,\eta,t) \tag{2.5}$$

at the front, and $q = q_\pm$ above and below it. An undisturbed front ($\eta = 0$) is characterised by a shelf in $\phi = \bar{\phi}(y)$ in geostrophic balance with a zonal jet $(u,v) = (\bar{u}(y),0)$, of maximum speed $\bar{u}(0) = c_- - c_+$, where $c_\pm = [\bar{\phi}(\pm\infty)]^{\frac{1}{2}}$ are the short-scale gravity wave speeds far from the front. Without loss of generality, we can take $f = 1$ and $c_+c_- = 1$ in the following. Since the flow decays exponentially away from the front, this implies $q_\pm = 1/c_\pm^2$.

Departing from earlier studies, we use the maximum Froude number $\mathsf{F} = \max[\bar{u}/\bar{\phi}^{\frac{1}{2}}]$ as the control parameter for the basic state flow. The maximum occurs at the front where $\mathsf{F} = c_- - c_+$, which we may take to be positive. Then the shallower fluid lies north of the front ($y > 0$). In terms of F, we have

$$c_\pm = (1 + \tfrac{1}{4}\mathsf{F}^2)^{\frac{1}{2}} \mp \tfrac{1}{2}\mathsf{F}. \tag{2.6}$$

The maximum Rossby number R occurs just on the shallow side of the front and is given by

$$\mathsf{R} = \mathsf{F}/c_+ = \mathsf{F}c_- . \tag{2.7}$$

Note also the inverse relationship, $\mathsf{F} = \mathsf{R}/\sqrt{1 + \mathsf{R}}$. In particular, $\mathsf{R} > 1$ corresponds to $\mathsf{F} > 1/\sqrt{2}$. For the non-rotating system, F becomes the Mach number for the analogous two-dimensional compressible flow equations. Hence, in the regime $\mathsf{F} > 1$, the flow is

susceptible to shock formation — particularly for short-scale disturbances which are not affected by rotation — in the full, nonlinear equations. Such phenomena would violate the hydrostatic approximation used to derive the shallow-water equations, and therefore we focus here on the regime $\mathsf{F} \leqslant O(1)$. As many geophysical flows are characterised by small R and F, this is not in fact a major restriction.

The basic-state flow has the form

$$\bar{\phi}(y) = c_\pm^2 \pm \mathsf{F}c_\pm \mathrm{e}^{-|y|/c_\pm} \quad \text{and} \quad \bar{u}(y) = \mathsf{F}\mathrm{e}^{-|y|/c_\pm} \tag{2.8}$$

(with $\bar{u} = -\mathrm{d}\bar{\phi}/\mathrm{d}y$, that is, in geostrophic balance). Linear stability is addressed by adding infinitesimal disturbances $\{\hat{u}(y), \hat{v}(y), \hat{\phi}(y)\}\mathrm{e}^{\mathrm{i}(kx-\sigma t)}$ and linearising the equations of motion about the basic state. Here k is the disturbance wavenumber and σ is the disturbance frequency (a positive imaginary part implying instability). We seek disturbances which do not change the basic-state PV (except through displacements of the front, cf. (2.5)). This amounts to replacing any one of the three equations (2.1)–(2.3) with

$$q\hat{\phi} = \mathrm{i}k\hat{v} - \hat{u}', \tag{2.9}$$

where $q = q_\pm = 1/c_\pm^2$ is the uniform PV either side of the front, and $'$ denotes $\mathrm{d}/\mathrm{d}y$. We obtain two other independent equations using (2.1) and (2.3),

$$\mathrm{i}(k\bar{u} - \sigma)\hat{u} + (\bar{u}' - 1)\,\hat{v} + \mathrm{i}k\hat{\phi} = 0, \tag{2.10}$$

$$\mathrm{i}(k\bar{u} - \sigma)\hat{\phi} + \mathrm{i}k\bar{\phi}\hat{u} + (\bar{\phi}\hat{v})' = 0. \tag{2.11}$$

These last three equations apply everywhere except at the front, $y = \eta(x, t) = \hat{\eta}\mathrm{e}^{\mathrm{i}(kx-\sigma t)}$. There, we linearise (2.5) to obtain

$$\mathrm{i}(k\mathsf{F} - \sigma)\hat{\eta} = \hat{v}(0) \tag{2.12}$$

using $\bar{u}(0) = \mathsf{F}$. Furthermore, boundary conditions are required to match the fields at $y = \eta$. (All fields are required to vanish as $y \to \pm\infty$.) Continuity of v at $y = \eta$ simplifies to continuity of $\hat{v}$ at $y = 0$. On the other hand, continuity of u involves a contribution from $\bar{u}(\eta) = \bar{u}(0) + \eta\bar{u}'(0^\pm) + O(\eta^2)$. But $\bar{u}'(0^\pm) = \mp\mathsf{F}/c_\pm$ is discontinuous because of the jump in PV. Hence, continuity of (total) u implies

$$\hat{u}(0^+) = \hat{u}(0^-) + (c_+ + c_-)\mathsf{F}\hat{\eta}. \tag{2.13}$$

Finally, continuity of ϕ simplifies to $\hat{\phi}(0^+) = \hat{\phi}(0^-)$ since $\bar{\phi}'$ is everywhere continuous. However, we do not need to enforce this explicitly as it is implied by (2.10) at $y = 0^\pm$ and (2.12). Hence, at $y = 0$, there are just three matching conditions, $\hat{v}(0^+) = \hat{v}(0^-)$, (2.12) and (2.13). From these, η can be eliminated, leaving just two conditions, which equals the total number of y derivatives on the disturbance fields in (2.9), (2.10) and (2.11).

2.2. *Numerical considerations*

The solution procedure follows in part Paldor (1983) and Boss *et al.*(1996), with some important differences. First, we substitute $\hat{w} = \mathrm{i}\hat{v}$ to factor out the dependence on i. As the non-constant coefficients in (2.9)–(2.11) involve only exponential functions, we seek

solutions of the form

$$\hat{u}(y) = c_{\pm} e^{-K^{\pm}|y|} \sum_{n=0}^{\infty} \hat{u}_n^{\pm} e^{-n|y|/c_{\pm}},$$

$$\hat{w}(y) = c_{\pm} e^{-K^{\pm}|y|} \sum_{n=0}^{\infty} \hat{w}_n^{\pm} e^{-n|y|/c_{\pm}},$$

$$\hat{\phi}(y) = c_{\pm}^2 e^{-K^{\pm}|y|} \sum_{n=0}^{\infty} \hat{\phi}_n^{\pm} e^{-n|y|/c_{\pm}}. \tag{2.14}$$

Then, equating coefficients of $e^{-\Omega_n^{\pm}|y|/c_{\pm}}$ for each n, where $\Omega_n^{\pm} \equiv c_{\pm}K^{\pm} + n$, we obtain the recurrence relations

$$k_{\pm}\hat{w}_n^{\pm} = \hat{\phi}_n^{\pm} \mp \Omega_n^{\pm}\hat{u}_n^{\pm}, \tag{2.15}$$

$$k_{\pm}\hat{\phi}_n^{\pm} - \sigma\hat{u}_n^{\pm} + \hat{w}_n^{\pm} = -\varepsilon_{\pm}(k_{\pm}\hat{u}_{n-1}^{\pm} \pm \hat{w}_{n-1}^{\pm}), \tag{2.16}$$

$$k_{\pm}\hat{u}_n^{\pm} - \sigma\hat{\phi}_n^{\pm} \pm \Omega_n^{\pm}\hat{w}_n^{\pm} = -\varepsilon_{\pm}(k_{\pm}\hat{\phi}_{n-1}^{\pm} \pm k_{\pm}\hat{u}_{n-1}^{\pm} + \Omega_n^{\pm}\hat{w}_{n-1}^{\pm}), \tag{2.17}$$

where $k_{\pm} \equiv kc_{\pm}$ are scaled wavenumbers, and $\varepsilon_{\pm} \equiv F/c_{\pm}$ are the local Rossby numbers at $y = 0^{\pm}$ (the larger being $\varepsilon_+ = \mathsf{R}$). When $n = 0$, the $n-1$ terms are absent, and solvability (for $k \neq 0$) requires

$$c_{\pm}K^{\pm} = \sqrt{k_{\pm}^2 + 1 - \sigma^2} \tag{2.18}$$

and $\hat{\phi}_0^{\pm} = \hat{u}_0^{\pm}(\sigma k_{\pm} \pm c_{\pm}K^{\pm})/(k_{\pm}^2 + 1)$. Note that $K^{\pm} = 0$ gives the dispersion relation for inertia-gravity waves far from the front.

Here, we do not yet know the value of σ, so a guess has to be made. In fact, there are an infinite number of possible modes, but only one has low frequency in the limit $\mathsf{F} \ll 1$ and corresponds to the balanced vortical mode. Anticipating this mode becomes unstable at sufficiently large F, we use the small F (or equivalently small R) 'quasi-geostrophic' approximation

$$\sigma = k\mathsf{F}[1 - (1 + k^2)^{-1/2}] + O(\mathsf{F}^2) \tag{2.19}$$

(cf. Nycander, Dritschel & Sutyrin 1991) as a first guess. It turns out that this is an excellent approximation for the mode frequency up to $\mathsf{F} = 2$.

We then take $\hat{u}_0^{\pm} = 1$ arbitrarily, and assign the corresponding values of $\hat{\phi}_0^{\pm}$ and $\hat{w}_0^{\pm}$. As the equations are linear, a constant factor can be included later to enforce the boundary conditions at $y = 0$. With these starting values and the guess for σ, (2.15)–(2.17) can be solved recursively for the higher-order coefficients. Here, we use 1000 coefficients, sufficient to ensure machine precision (at quadruple precision) except when $\mathsf{R} \gtrsim 1$, see below. Then, the series in (2.14) are summed at $y = 0$ to obtain $\hat{u}(0^{\pm})$, $\hat{w}(0^{\pm})$ and $\hat{\phi}(0^{\pm})$. First, $\hat{w}$ is made continuous by multiplying $\hat{u}(0^-)$, $\hat{w}(0^-)$ and $\hat{\phi}(0^-)$ by $\lambda = \hat{w}(0^+)/\hat{w}(0^-)$. Next, $\hat{\eta}$ is found from (2.13). Finally, a *new* guess for σ is found by substituting this value of $\hat{\eta}$ into (2.12). If the new guess differs by more than a tolerance, here 10^{-25}, from the previous one, the above procedure is repeated. Remarkably, this very simple procedure converges exponentially fast over the whole parameter space investigated.

When $\mathsf{R} \geqslant 1$, one can demonstrate that the series on the shallow side ($y > 0$) diverges near the front. In this regime, Boss *et al.*(1996) solved the linear equations for all $y > 0$ by numerical integration (using the variable $z = e^{-y/c_+}$). However, the series converges fast for sufficiently large y, and hence it is necessary to perform a numerical integration only over a small range in y typically. The series diverges when the local Rossby number
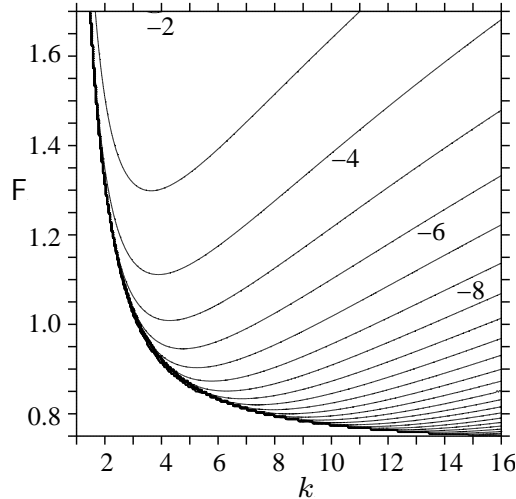
FIGURE 2. Growth rate contours — of $\log_{10}(\sigma_i)$ — in the k-F parameter plane. A few contours are labelled (the contour interval is 1).

$\mathrm{Re}^{-y/c_+} \geqslant 1$. Convergence slows as $\mathsf{R} \to 1$, so for $\mathsf{R} > 0.9$, we use the series only beyond $y = Y_+$, with Y_+ chosen so that the local Rossby number there equals 0.7. From $y = Y_+$ to 0, numerical integration using a 4th-order Runge-Kutta method is used, with a step size $\Delta y \leqslant 10^{-4} c_+ / \max(k, 1)$. These numerical values were chosen by trial and error to ensure both solution methods (series only and series plus numerical integration) at $\mathsf{R} = 0.9$ agree to at least 7 digits in their value of σ over $0 < k < 10$. The results reported are insensitive to these parameters except for very small $\mathsf{R} - 1$, when growth rates can be of the order of the machine precision.

3. Numerical results

We start by examining the general stability properties over the complete parameter space investigated, namely $1 \leqslant k \leqslant 16$ and $0.75 \leqslant \mathsf{F} \leqslant 1.7$ (or, alternatively $1.08 \leqslant \mathsf{R} \leqslant 3.68$). Figure 2 shows the growth rate

$$\sigma_i = \mathrm{Im}\,(\sigma),$$

in logarithmic scale, in the k-F plane. First of all, there is a long-wave cutoff: only wavenumbers larger than some cutoff wavenumber k_c are unstable according to the numerics (we cannot discount other modes of instability, but an extensive search has not revealed any). The long-wave cutoff increases rapidly as $\mathsf{F} \to 1/\sqrt{2}$ or $\mathsf{R} \to 1$, and the growth rates fall sharply. Even quadruple precision is not enough to capture the exceedingly weak growth rates below $\mathsf{F} = 0.73$, but their existence is clear from the asymptotic analysis described in the next section. Remarkably, growth rates are very small, indeed never greater than 7.76×10^{-6}, when $\mathsf{F} \leqslant 1$. These instabilities would be virtually impossible to detect in numerical simulations of the full equations, and would likely be overwhelmed by nonlinear effects (see discussion).

Instability occurs when the frequency of the (PV-controlled) Rossby wave which, in the first instance, we may approximate by the quasi-geostrophic result (2.19), $\sigma_R = k\mathsf{F}[1 - (1 + k^2)^{-1/2}]$, matches (or nearly matches) that of an inertia-gravity wave on the shallow side of the front, $\sigma_G = (1 + c_+^2(k^2 + \ell^2))^{1/2}$, where ℓ is the y wavenumber far from the front; see figure 3. When $\mathsf{F} < 1/\sqrt{2}$, no real values of k and ℓ can be found for which

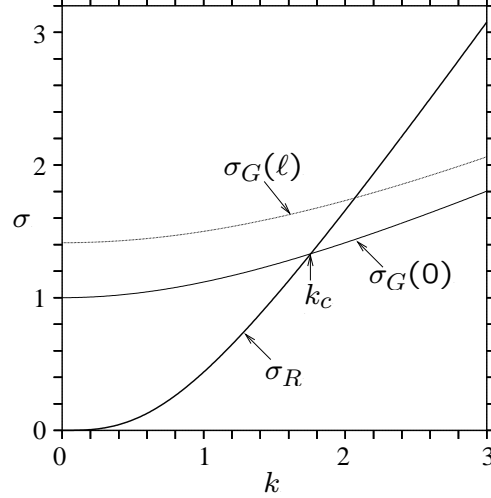FIGURE 3. Approximate Rossby-wave σ_R and gravity-wave σ_G dispersion relations as a function of x wavenumber k. σ_R makes use of the quasi-geostrophic (QG) approximation (strictly valid for $\mathsf{R} \ll 1$), while σ_G applies far from the front on the shallow side. $\sigma_G(0)$ is for a y wavenumber $\ell = 0$, while $\sigma_G(\ell)$ is for finite ℓ (here 2). The curves were generated using $\mathsf{R} = 3$ ($\mathsf{F} = 1.5$). The predicted long-wave cutoff occurs when $\sigma_R = \sigma_G(0)$, at $k = k_c$. For all $k > k_c$ there exists a real value of ℓ for which $\sigma_R = \sigma_G(\ell)$, and there is always instability. Note: the curves cross only when $\mathsf{R} > 1$.

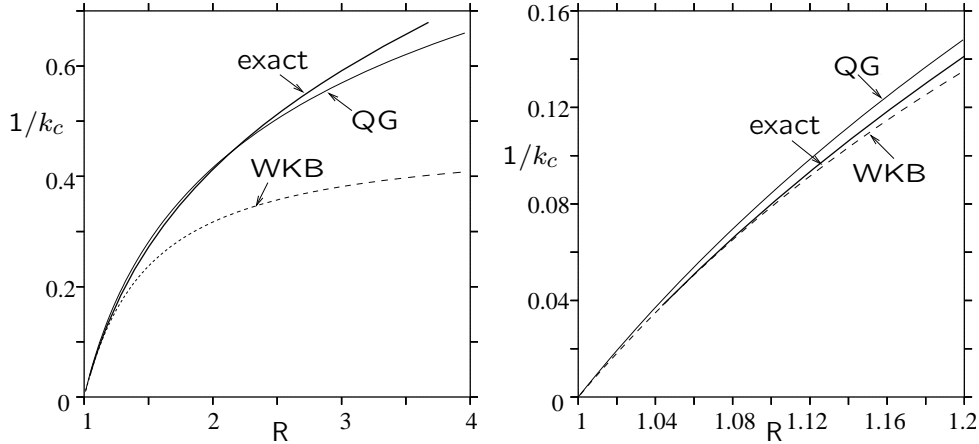FIGURE 4. Approximate quasi-geostrophic (QG) estimate of the long-wave cutoff (or its inverse $1/k_c$) compared with the 'exact' stability analysis for Rossby numbers (a) $1 \leqslant \mathsf{R} \leqslant 4$ and (b) an enlargement for $1 \leqslant \mathsf{R} \leqslant 1.2$. Note that the QG model is strictly valid only when $\mathsf{R} \ll 1$ ($\mathsf{F} > 1/\sqrt{2}$). Also shown is the WKB estimate, (4.17) of §4.

$\sigma_R = \sigma_G$. However, for $\mathsf{F} \geqslant 1/\sqrt{2}$, there exists a range of k extending from a long-wave cutoff k_c to ∞ and real values of $\ell(k)$ with matching frequencies. Moreover, there is then a turning point where the phase speed σ/k matches the Doppler-shifted frequency of the inertia-gravity wave $k(\bar{u} + \bar{\phi}^{1/2})$. Through this turning point, the character of the mode changes from an evanescent Rossby mode to an oscillatory (but slowly decaying) inertia-gravity mode; this is discussed further in §4.

This qualitative picture is consistent with the numerical results, as demonstrated next. The long-wave cutoff k_c is found to coincide with $\ell = 0$, i.e. an infinitely long wave in y (or equivalently a turning point for $y \to \infty$). Using $\sigma_R = \sigma_G$ for $\ell = 0$ then gives a
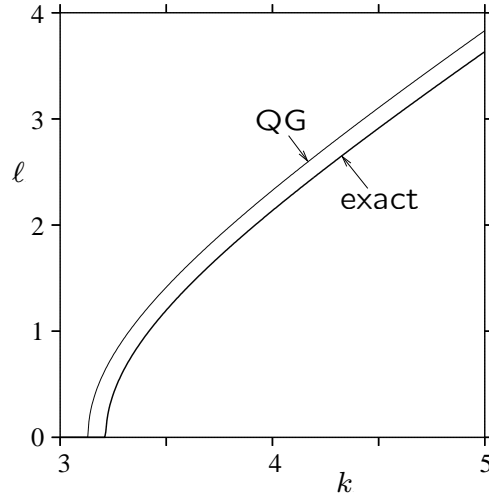
D. G. Dritschel & J. Vanneste

FIGURE 5. Approximate quasi-geostrophic (QG) estimate of the y wavenumber ℓ compared with the 'exact' stability analysis as a function of k. Here, we have taken $\mathsf{F} = 1$ ($\mathsf{R} = 1.618...$). Maximum instability is observed for $k = 4.3386$. Note that ℓ is real only for $k \geqslant k_c$.

relation between k_c and either R or F. This is compared in figure 4 against the numerical results (i.e. the 'exact' or full stability analysis). The agreement is spectacular considering the fact that the QG approximation is being pushed well beyond its expected limits of validity. In fact, the agreement remains good for R as large as 3. As $\mathsf{R} \to 1$, the predicted k_c is given by $1/(\mathsf{R} - 1)$. This result is very close to the exact value: the asymptotic calculations of §4 show that the exact value tends to $k_c = 1.0606/(\mathsf{R} - 1)$.

The agreement also confirms the simple idea that instability can be predicted by matching the frequencies of Rossby and gravity modes. This idea can also be used to estimate the dependence of the y wavenumber ℓ on k, shown in figure 5 for the case $\mathsf{F} = 1$ ($\mathsf{R} = 1.618...$). Here, the 'exact' results are obtained from the imaginary part of K^+, see (2.14), since for $y \gg 1$, the disturbance $(\hat{u}, \hat{w}, \hat{\phi}) \sim (\hat{u}_0^+, \hat{w}_0^+, \hat{\phi}_0^+)e^{-K^+ y}$. Hence, $\ell = -\mathrm{Im}\,(K^+)$. The agreement is excellent, apart from a small offset in k. Again this shows that mode matching explains the essential nature of the instability.

The real part of K^+ must be positive for the disturbance to decay as $y \to \infty$. This is shown for the same case ($\mathsf{F} = 1$) in figure 6, now using the full stability analysis. Instability erupts at $k = k_c = 3.21445...$, and for the entire unstable range $K_r^+ > 0$. However, K_r^+ is $O(\sigma_i) \ll 1$, so the decay is extremely slow (but nonetheless exponential). Over any reasonable distance, the disturbance on the shallow side of the front looks like a pure gravity wave (and that on the deep side looks like a decaying Rossby wave). As k passes downward through k_c, it appears that K_r^+ jumps to a large value. Closer inspection (figure 6, right panel) reveals that K_r^+ is in fact continuous, as is the y wavenumber $\ell = -K_i^+$ (this is zero for $k \leqslant k_c$). Hence, there is a continuous transition to instability, and all unstable modes are found to have finite energy.

4. WKB analysis

In the limit of large wavenumber $k \gg 1$, the instability can be studied asymptotically using a WKB approach, following Ford (1993, 1994). The results are most useful in the marginally-unstable regime $\mathsf{R} \to 1$, when the largest growth rates occur for $k \gg 1$. We now derive WKB approximations for the frequency σ of the unstable mode, including
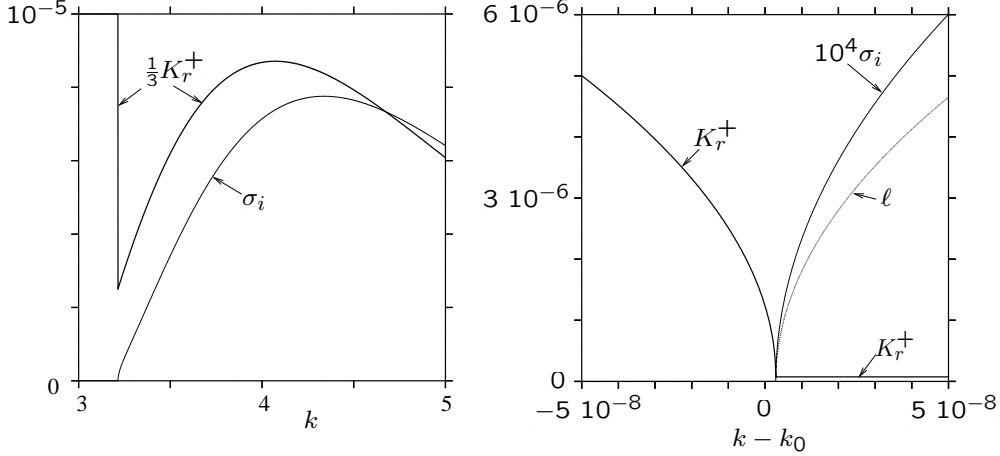
FIGURE 6. Dependence of K_r^+ (the real part of K^+) and the growth rate σ_i on k for $\mathsf{F} = 1$ ($\mathsf{R} = 1.618...$). The left panel shows a range of k including the long-wave cutoff and the peak instability. The right panel, centred on $k_0 = 3.21445147$, focuses on the region of the long-wave cutoff; it also shows $\ell = -K_i^+$.

its exponentially small imaginary part. We only sketch the derivation and relegate the details to Appendix A.

From (2.9)–(2.11), a single equation for $\hat{u}$ can be derived. This reads

$$\hat{u}'' + \frac{\bar{\phi}'}{\bar{\phi}}\hat{u}' + \left[k^2 \left(\frac{\bar{c}^2}{\bar{\phi}} - 1 \right) - \frac{\bar{\phi}}{c_\pm^4} + \frac{(\bar{\phi}\bar{c})'}{c_\pm^2 \bar{\phi}} \right] \hat{u} = O(1/k), \tag{4.1}$$

where $\bar{c} = c - \bar{u} = \sigma/k - \bar{u}$. The associated boundary condition is deduced from (2.12)–(2.13) and may be written in the form

$$-\mathrm{i} \left[k\bar{c}\frac{\hat{u}}{\hat{v}} \right]_{0^-}^{0^+} = \mathsf{F}(c_+ + c_-), \quad \text{with} \quad \hat{v} = \frac{-\mathrm{i}}{k} \left(\hat{u}' + \bar{c}\hat{u} \right) + O(1/k^2). \tag{4.2}$$

Note that the error terms in (4.1)–(4.2) assume that $\hat{u}'/\hat{u} = O(k)$, as is relevant for the WKB solution.

We seek solutions to (4.1)–(4.2) for $k \gg 1$ in the form

$$\hat{u} = \mathcal{A}(y)\mathrm{e}^{k\Psi(y)}, \tag{4.3}$$

and require that both $(\mathcal{A}, \Psi)$ and $(\mathcal{A}, -\Psi)$ be solutions. This leads to the two equations (A 1)–(A 2) for $\mathcal{A}$ and Ψ. The first equation can be solved perturbatively, by expanding

$$\Psi = \Psi_0 + \Psi_1/k + O(1/k^2) \quad \text{and} \quad c = \mathsf{F} + c_1/k + c_2/k^2 + O(1/k^3). \tag{4.4}$$

At leading order, this gives

$$\Psi_0' = \mp \left(1 - \frac{\bar{c}_0^2}{\bar{\phi}} \right)^{1/2}, \quad \text{where} \quad \bar{c}_0 = \mathsf{F} - \bar{u}(y),$$

and the signs, corresponding to $y \gtrless 0$, are chosen to ensure exponential decay away from the PV jump. Introducing this result into (4.2) readily gives

$$c_1 = -\mathsf{F}(c_+ + c_-)/2 = -\mathsf{F}(1 + \mathsf{F}^2/4)^{1/2}. \tag{4.5}$$

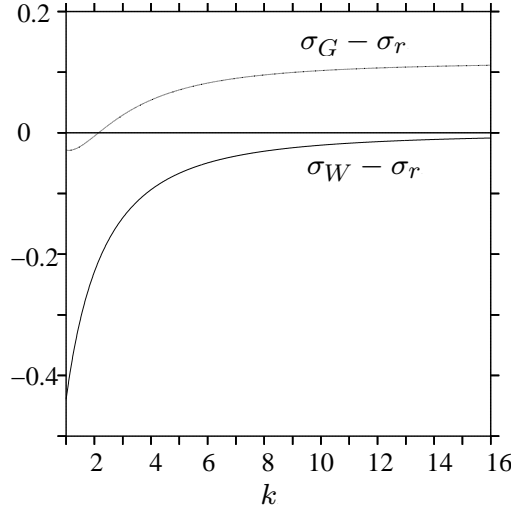In Appendix A, we carry out the calculation to the next order and find that $c_2 = 0$.

FIGURE 7. Difference between the WKB frequency and the 'exact' frequency, $\sigma_W - \sigma_r$, and between the QG frequency and the 'exact' frequency, $\sigma_G - \sigma_r$, for $\mathsf{F} = 1$. Note $\sigma_r = 14.89...$ for $k = 16$.

Thus, for large k, the Rossby-wave frequency is given by

$$\sigma = k\mathsf{F} - \mathsf{F}(1 + \mathsf{F}^2/4)^{1/2} + O(1/k^2), \tag{4.6}$$

consistent with the quasi-geostrophic approximation (2.19) in the limit $\mathsf{F} \to 0$. Figure 7 shows how this estimate (denoted σ_W in the figure) compares with the actual real part of σ, for $\mathsf{F} = 1$ and over the same range of wavenumbers used in figure 2. A comparison with the QG estimate (denoted σ_G) is also given. At large k, the WKB estimate is more accurate, as would be expected.

The computation leading to (4.6) can in principle be extended to obtain approximations to σ accurate to higher orders $O(1/k^n)$. To all algebraic orders σ is real, because, as recognised by Ford (1993; see also Knessl & Keller 1992), the instability is characterised by a non-zero imaginary part of σ that is exponentially small in k. This can be traced to the existence, ignored in the above developments, of a turning point where Ψ changes from being purely real to being purely imaginary. To leading order, the turning point position, y_* say, is determined by the condition

$$\bar{c}_0^2(y_*) = [\mathsf{F} - \bar{u}(y_*)]^2 = \bar{\phi}(y_*), \tag{4.7}$$

which has a solution $y_* > 0$ for $\mathsf{R} > 1$. This condition expresses the match at y_* between the leading-order Rossby-wave frequency $k\mathsf{F}$ and the Doppler-shifted gravity-wave frequency $k(\bar{u} + \bar{\phi}^{1/2})$.

The instability growth rate $\sigma_i = \text{Im}(\sigma)$ can be estimated by modifying the WKB solution on the shallow side of the front $y > 0$ to account for the existence of this turning point. Briefly, the decaying solution (4.3) must be supplemented by an exponentially growing solution, which is subdominant for $0 < y < y_*$, but becomes of a similar order as the decaying solution for $y \approx y_*$. The combination of the two solutions, with appropriate relative amplitudes, ensures that the oscillatory solution for $y > y_*$ satisfies a radiation boundary condition as $y \to \infty$. Note that the exponential decay of the solutions for $y \to \infty$ with decay rate proportional to σ_i described in §3 is not apparent in the solution for $\hat{u}$ so obtained; this is because the WKB analysis implicitly assumes that $y \ll \sigma_i^{-1}$.

In Appendix A, we derive several approximations to σ_i, valid in regions of parameter

space distinguished by the relative values of $k \gg 1$ and

$$\delta \equiv \mathsf{R} - 1 > 0.$$

Assuming that $k \gg 1$, we obtain the expression

$$\sigma_i \sim \mathsf{F} \frac{c_+ + c_-}{4} \mathrm{e}^{-2k\Psi_*}, \quad \text{where} \quad \Psi_* = \int_0^{y_*} \left(1 - \frac{\bar{c}^2}{\bar{\phi}}\right)^{1/2} \mathrm{d}y, \tag{4.8}$$

and c is approximated as $c \sim \mathsf{F} + c_1/k$, with c_1 given in (4.5). This result is valid uniformly for $k \gg 1$ in two regimes: (i) $\delta = O(1)$, and (ii) $\delta = O(1/k) \ll 1$. In regime (i), Ψ_* can be expanded in inverse powers of k to find

$$\Psi_* = \int_0^{y_*} \left(1 - \frac{\bar{c}_0^2}{\bar{\phi}}\right)^{1/2} \mathrm{d}y - \frac{1}{k} \int_0^{y_*} \frac{\bar{c}_0 c_1}{\bar{\phi}(1 - \bar{c}_0^2/\bar{\phi})^{1/2}} \, \mathrm{d}y + O(1/k^2). \tag{4.9}$$

This is the result originally obtained by Ford (1993). It fails in regime (ii) because for sufficiently large $y < y_*$, $1 - \bar{c}_0^2/\bar{\phi} = O(\delta)$ and the expansion leading to (4.9) becomes disordered.

In regime (ii), since $k\delta = O(1)$, it is natural to introduce the scaled, dimensionless wavenumber

$$\kappa \equiv \delta c_+ k = O(1). \tag{4.10}$$

Noting that

$$\mathsf{F} = \frac{1}{\sqrt{2}} + \frac{3}{4\sqrt{2}} \delta + O(\delta^2), \tag{4.11}$$

and expanding equation (4.7) for the turning-point position gives

$$z_* \equiv \mathrm{e}^{-y_*/c_+} = \frac{2\delta}{3} \left(1 - \frac{3}{4\kappa}\right) + O(\delta^2). \tag{4.12}$$

Thus, there is a turning point and hence instability is possible provided that $\kappa > 3/4$. Taking (4.10)–(4.11) into account, this gives a first WKB approximation to the cutoff wavenumber

$$k_c = \frac{3\sqrt{2}}{4\delta} + O(1). \tag{4.13}$$

This result is refined below with the calculation of the $O(1)$ term. After introducing (4.10) and (4.11), (4.8) reduces to

$$\sigma_i \sim \frac{3}{8} \mathrm{e}^{-2k\Psi_*}, \tag{4.14}$$

where Ψ_* is expanded in powers of δ according to

$$2k\Psi_* = \frac{a_1}{\delta} + \frac{a_2}{\delta^{1/2}} + a_3 + O(\delta^{1/2}). \tag{4.15}$$

Here a_1, a_2 and a_3 are functions of κ defined by integrals and given by $a_1 = 5.782\,\kappa$, $a_2 = -\pi[2\kappa(4\kappa - 3)]^{1/2}$, and $a_3 = 7.052\,\kappa - 3.789$. (See (A 9)–(A 11) for the exact expressions of the numerical constants given here to 4-digit accuracy.)

As the expression for a_2 suggests, the approximation (4.14)–(4.15) breaks down for $\kappa - 3/4 = O(\delta)$, i.e. in the vicinity of the cutoff wavenumber. Since this is also where the maximum of σ_i is attained, it is important to derive an asymptotic formula appropriate for this regime, which we denote by (iii) and is defined in dimensional terms by $k - 3\sqrt{2}/(4\delta) = O(1)$.

Calculations detailed in Appendix A examine the instability in regime (iii). There we start by defining the scaled wavenumber

$$\mathsf{k} \equiv \frac{\kappa - 3/4}{\delta} = O(1) \qquad (4.16)$$

and show that instability occurs only for $\mathsf{k} > 31/24$. This provides the estimate of the cutoff wavenumber

$$k_c = \frac{3\sqrt{2}}{4\delta} + \frac{71\sqrt{2}}{48} + O(\delta), \qquad (4.17)$$

which improves on (4.13). (This estimate is compared with the numerical and quasi-geostrophic results in figure 4.) The instability growth rate is then found in the form

$$\sigma_i \sim \frac{3}{4} \sinh(\pi\nu) \mathrm{e}^{-2\Phi_*/\delta}, \qquad (4.18)$$

where

$$\nu = (6\mathsf{k} - 31/4)^{1/2} \quad \text{and} \quad 2\Phi_* = b_1 + \delta b_2 + O(\delta^2).$$

Here $b_1 = 4.336$ and $b_2 = 5.782\mathsf{k} + 1.5$ are defined by integrals given in (A 21)–(A 22). In particular, the maximum growth rate is achieved for $\mathsf{k} = 1.735$. Note that the two approximations (4.14) and (4.18) can be verified to match in the intermediate region $\delta \ll |\kappa - 3/4| \ll 1$ where both are valid.

The three growth-rate estimates (4.8), (4.14) and (4.18), denoted by WKB_1, WKB_2 and WKB_3, respectively, are compared in figure 8 with the 'exact' growth rate as a function of κ and for two values of F. For the case $\mathsf{F} = 0.8$ ($\delta = \mathsf{R} - 1 = 0.1816\ldots$, top panels), the estimate (4.8) accurately captures the exponential decay of σ_i for large κ. It also performs reasonably well for $\kappa = O(1)$ and away from the long-wave cutoff; this is the range for which it overlaps with (4.14). The performance of the third estimate (4.18) is best appreciated from the top right panel which focuses on the region near the cutoff wavenumber and maximum growth rate. The estimate provides a good approximation to the cutoff wavenumber, but only a crude one for the behaviour of σ_i near its maximum. The situation improves as δ decreases. This is apparent from the results obtained for $\mathsf{F} = 0.76$ ($\delta = 0.1018\ldots$) shown in the bottom panel of figure 8. This time, (4.18) estimates well the long-wave cutoff ($\kappa_c = 0.88152...$ versus $0.86513...$) and provides the growth rate within a factor of approximately four. Convergence of (4.18) to the exact values of σ_i with $\delta \to 0$ appears to be very slow, and the limitations of quadruple precision forbid using a value of δ small enough to demonstrate it plainly. The slow convergence is well illustrated by the fact that values as small as $\delta = 10^{-9}$ are necessary to observe the overlap between (4.8) (or (4.14)) and (4.18) in their region of common asymptotic validity.

5. Discussion

This paper has re-examined the stability of a potential-vorticity front in the rotating shallow-water equations. This was previously examined by Ford (1993) and Boss *et al.*(1996). The front, whose properties depend on a single dimensionless parameter F (or equivalently R), is unstable provided that $\mathsf{F} > 1/\sqrt{2}$ (or $\mathsf{R} > 1$). The associated disturbances have Rossby-wave characteristics near the front and inertia-gravity-wave characteristics far away, on the shallow side of the front. The instability is exceptionally weak, with growth rates scaling exponentially in $1/(\mathsf{R} - 1)$ as $\mathsf{R} \to 1$ and numerically very small even for $\mathsf{R} - 1 = O(1)$. Correspondingly, the amplitude of the growing mode decays very slowly with the distance from the front.

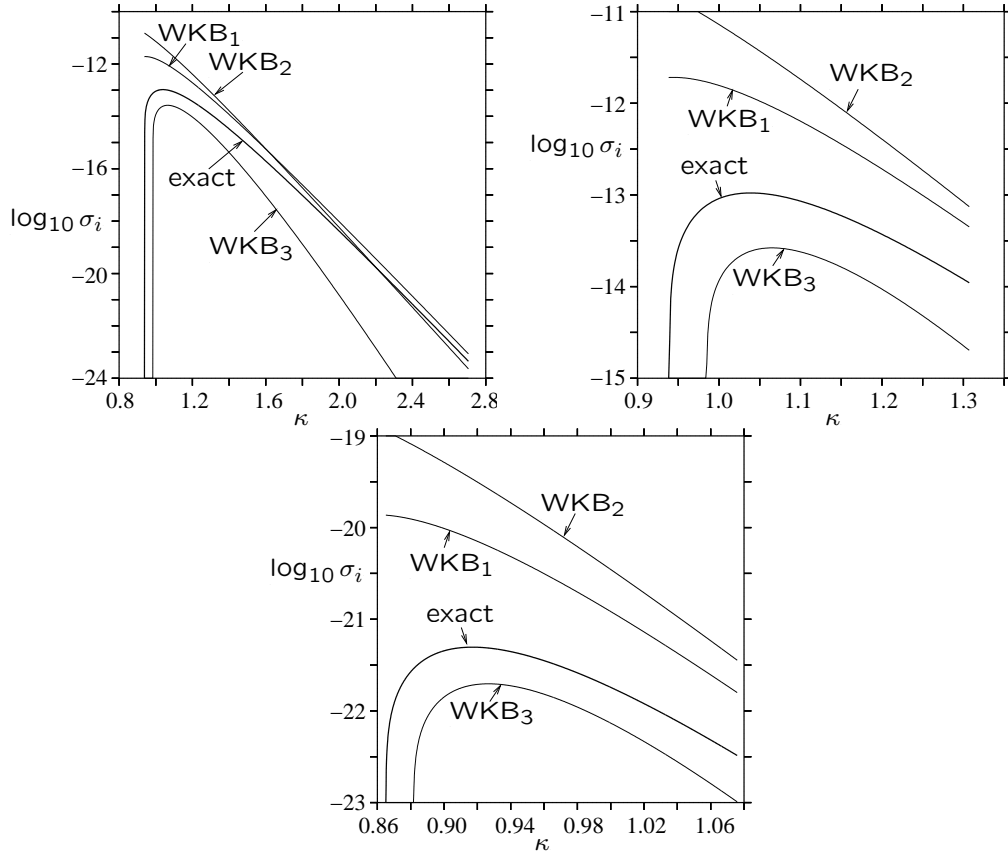The characteristics of the instability (y-wavenumber ℓ, cutoff wavenumber k_c) can

FIGURE 8. Comparison of various WKB estimates of the growth rate σ_i with the 'exact' result, as a function of the scaled wavenumber κ, for $\mathsf{F} = 0.8 \, (\mathsf{R} = 1.1816\ldots)$ (top panels) and $\mathsf{F} = 0.76 \, (\mathsf{R} = 1.1018\ldots)$ (bottom panel). The labels WKB_1, WKB_2 and WKB_3 correspond to formulas (4.8), (4.14) and (4.18), respectively.

be inferred from the condition of frequency matching between the near-front Rossby wave, and the far-field inertia-gravity wave. Whilst the dispersion relation of the latter is given explicitly (since the basic-flow height is constant in the far field), the Rossby-wave dispersion relation needs to be approximated in some way. The quasi-geostrophic approximation (2.19), which formally assumes $\mathsf{R} \ll 1$, turns out to be useful for this purpose since it proves remarkably accurate well into the unstable regime $\mathsf{R} > 1$. An asymptotically consistent alternative is provided by the WKB approximation (4.6) valid for $k \gg 1$. This approximation makes it possible to describe analytically the instability, including the long-wave cutoff, in the limit $\mathsf{R} \to 1$, when all the unstable wavenumbers satisfy $k = O(1/(\mathsf{R} - 1)) \gg 1$.

The instability studied in this paper illustrates several aspects of the concept of balance for rapidly rotating fluids. First, the observed stability in the regime $0 < \mathsf{R} < 1$ is consistent with the idea that a balanced flow, represented here by the frontal Rossby wave, is isolated from the inertia-gravity waves when a complete frequency separation exists. Second, the threshold value $\mathsf{R} = 1$ for instability coincides precisely with the breakdown of the frequency separation. Third, the unbalanced phenomenon — here the instability — is exponentially weak in the limit of small frequency overlap, and turns out to remain weak over a wide parameter range. This last point echoes what is frequently

observed in more realistic flows, namely the weakness of unbalanced phenomena even in the absence of a frequency separation.

In realistic, nonlinear, time-dependent flows, there is of course no frequency separation, and the excitation of inertia-gravity waves can be expected to take place for all values of R. The mechanism for this excitation can be either an instability of a type generalising that studied in this paper, or a spontaneous-adjustment mechanism similar to that examined by Vanneste & Yavneh (2004) and Vanneste (2004) in simple toy models. In a more realistic context, the nonlinear evolution of a potential-vorticity front in the full shallow-water equations would seem an ideal problem to examine this excitation. However, based on preliminary numerical simulations, even this simplest of problems appears formidable, requiring highly-accurate numerics as well as a careful initialisation to avoid a significant presence of inertia-gravity waves from the start. For small R, it is practically impossible to differentiate inertia-gravity waves from numerical error, even when numerical methods specifically designed to handle potential vorticity discontinuities are employed (cf. Mohebalhojeh & Dritschel (2001) and references). For larger R, it becomes increasingly difficult to separate balanced and unbalanced motions, and for $R > \sqrt{2}$, the governing equations themselves may break down as a result of shock formation (thereby violating the underlying hydrostatic approximation). In a way, these difficulties emphasise the tight control often exerted by balanced motions in geophysical flows.

Appendix A. WKB derivation

In this Appendix, we provide some details of the derivation of the approximations (4.6) for the Rossby-wave frequency, and (4.8), (4.14) and (4.18) for the instability growth rate.

A.1. *Rossby-wave frequency*

Introducing the WKB solution (4.3) into (4.1) leads to

$$k^2 \Psi'^2 \mathcal{A} + \mathcal{A}'' + \frac{\bar{\phi}'}{\bar{\phi}} \mathcal{A}' + \left[k^2 \left(\frac{\bar{c}^2}{\bar{\phi}} - 1 \right) - \frac{\bar{\phi}}{c_\pm^4} + \frac{(\bar{\phi}\bar{c})'}{c_\pm^2 \bar{\phi}} \right] \mathcal{A} = O(1/k), \qquad (A\,1)$$

$$2k\Psi' \mathcal{A}' + k\Psi'' \mathcal{A} + k\frac{\bar{\phi}'}{\bar{\phi}} \Psi' \mathcal{A} = O(1/k). \qquad (A\,2)$$

Expanding Ψ and c according to (4.4) gives

$$\Psi_0' = \mp \left(1 - \frac{\bar{c}_0^2}{\bar{\phi}} \right)^{1/2}, \quad \text{and} \quad \Psi_1' = -\frac{\bar{c}_0 c_1}{\bar{\phi}(1 - \bar{c}_0^2/\bar{\phi})^{1/2}}. \qquad (A\,3)$$

In particular,

$$\Psi_0' = \mp 1, \quad \Psi_0'' = 0 \quad \text{and} \quad \Psi_1' = 0 \quad \text{at} \quad y = 0^\pm. \qquad (A\,4)$$

It follows from (4.2), (4.3) and (A 2) that

$$\hat{v} = -\mathrm{i} \left[\Psi_0' + \frac{1}{k}\Psi_1' - \frac{1}{2k} \left(\frac{\Psi_0''}{\Psi_0'} + \frac{\bar{\phi}'}{\bar{\phi}} \right) + \frac{\bar{c}_0}{k c_\pm^2} \right] \hat{u} + O(1/k^2),$$

and hence that

$$\hat{v} = \mathrm{i} \left(\pm 1 - \frac{\mathsf{F}}{2k} \right) \hat{u} + O(1/k^2) \quad \text{at} \quad y = 0^\pm. \qquad (A\,5)$$

Introducing (A 4) and (A 5) into (4.2) leads to the first two corrections in the asymptotic expansion of c, namely $c_1 = -\mathsf{F}(c_+ + c_-)/2$ and $c_2 = 0$, and hence to the approximation

(4.6) for the frequency. Note that this approximation provides one more term (which turns out to vanish) than that given by Ford (1993, 1994); as will be seen below, this higher accuracy is necessary to obtain an approximation for the maximum growth rate and cutoff wavenumber in the limit $R \to 1$.

A.2. *Growth rate in regimes (i) and (ii)*

As described in §4, the instability is associated with the existence of a turning point y_* satisfying (4.7). Because of this turning point, we must consider a superposition of growing and decaying WKB solutions for $y > 0$. In regime (i), defined by $k(R-1) \gg 1$ and considered by Ford (1993), the WKB solution corresponding to (A 3) remains valid for $y_* - y \gg k^{-2/3}$. Taking

$$\Psi_0 = \int_0^y \left(1 - \frac{\bar{c}_0^2(y')}{\bar{\phi}(y')}\right)^{1/2} \mathrm{d}y' \quad \text{and} \quad \Psi_1 = -\int_0^y \frac{\bar{c}_0(y')c_1}{\bar{\phi}(y')[1 - \bar{c}_0^2(y')/\bar{\phi}(y')]^{1/2}} \, \mathrm{d}y',$$

the solution in this range is written as

$$u = \mathcal{A}(y) \left[a e^{k\Psi_0 + \Psi_1} + b e^{-k\Psi_0 - \Psi_1}\right] + O(1/k),$$

for two constants a and b. The Airy-function connection with an outward-propagating solution for $y - y_* \gg k^{-2/3}$ imposes the relationship

$$\frac{a e^{k\Psi_0(y_*) + \Psi_1(y_*)}}{b e^{-k\Psi_0(y_*) - \Psi_1(y_*)}} = \frac{\mathrm{i}}{2} \tag{A 6}$$

(Ford 1993, 1994; see also, e.g., Bender & Orszag 1991, §10). It then follows from (4.2) that

$$\hat{v} = -\mathrm{i}\Psi_0' \left(a e^{k\Psi_0 + \Psi_1} - b e^{-k\Psi_0 - \Psi_1}\right) + O(1/k)$$

and

$$c_1 \left(1 + \frac{1 + a/b}{1 - a/b}\right) = -F(c_+ + c_-). \tag{A 7}$$

Using (A 6) and the smallness of the exponentials gives

$$\operatorname{Im} c_1 = \frac{F(c_+ + c_-)}{4} e^{-2[k\Psi_0(y_*) + \Psi_1(y_*)]}, \tag{A 8}$$

that is, the estimate (4.8) for the growth rate, with Ψ_* approximated as in (4.9).

The WKB approach just outlined breaks down when $k(R-1) = O(1)$. To estimate the growth rate in this regime, denoted by (ii), a different WKB expansion can be used, with $\delta = R - 1$ as the small parameter. An alternative is to note that the derivation above remains valid in regime (ii) provided that one avoids introducing the expansion

$$\frac{\bar{c}^2}{\bar{\phi}} - 1 = \frac{\bar{c}_0^2}{\bar{\phi}} - 1 + \frac{2\bar{c}_0 c_1}{k\bar{\phi}} + O(1/k^2).$$

Repeating the derivation leading to (A 8) but without this expansion (and with c approximated by $F + c_1/k$ and c_1 given in (4.5)) leads to the growth rate in the form (4.8). This approximation is valid uniformly for both regimes (i) $\delta = O(1)$ and (ii) $\delta = O(1/k)$. The simplified expression (4.9) follows in regime (i) by expansion in inverse powers of k. We now derive a simplified expression valid in regime (ii) by expansion in powers of δ.

We first note that the prefactor $F(c_+ + c_-)/4$ in (4.8) reduces to $3/8$ (cf. (4.14)). Then, using (4.10)–(4.12), we compute

$$\frac{c}{c_+} = 1 + \delta \left(1 - \frac{3}{4\kappa}\right) + O(\delta^2)$$

and

$$1 - \frac{\bar{c}^2}{\bar{\phi}} = \frac{z(3-z)}{1+z} - \delta \frac{2(1-z^2)(1-z-3/(4\kappa)) - z(1-z)^2}{(1+z)^2} + O(\delta^2),$$

where $z \equiv \exp(-y/c_+)$. Substituting into (A 2) and changing the variable of integration from y to z leads to an integral that is best expanded by splitting the integration range $[z_*, 1]$ at some intermediate $z_* \ll z \ll 1$ (e.g. Hinch 1991, §3.4). A tedious but straightforward computation leads to the approximation (4.15), where

$$a_1 = 2\kappa \int_0^1 \left(\frac{3-z}{z(1+z)} \right)^{1/2} dz \qquad (A\,9)$$

$$a_2 = -\pi[2\kappa(4\kappa - 3)]^{1/2} \qquad (A\,10)$$

$$a_3 = \kappa \left[\frac{4}{\sqrt{3}} - \int_0^1 \left(\frac{(z-1)(z^2+z-2)}{z^{3/2}(1+z)^{3/2}(3-z)^{1/2}} - \frac{2}{\sqrt{3}z^{3/2}} \right) dz \right]$$
$$- \frac{3}{\sqrt{3}} - \frac{3}{2} \int_0^1 \left(\frac{z^2-1}{z^{3/2}(1+z)^{3/2}(3-z)^{1/2}} + \frac{1}{\sqrt{3}z^{3/2}} \right) dz. \qquad (A\,11)$$

The same result obtains if (4.1) is expanded for $\delta \ll 1$, $\kappa = O(1)$, and a WKB-analysis of the resulting equation is performed. The derivation is then particularly tedious because approximations in four distinct regions ($z = O(1)$, $z_* < z = O(\delta)$, $|z - z_*| = O(\delta^{1/3})$, and $z < z_*$) must be matched.

A.3. *Growth rate in regime (iii)*

In an $O(\delta)$ neighbourhood of the cutoff wavenumber $\kappa = 3/4 + O(\delta)$, the WKB approximation used above breaks down. This is because for $y \gg 1$, $k^2(1 - \bar{c}_0^2/\bar{\phi}) = O(1)$, and the other terms multiplying $\hat{u}$ in (4.1) must be taken into account. The turning point satisfies $z_* = O(\delta^2)$ and two expansions must be derived and matched: the first one valid for $z = O(1)$, the second valid for $z = O(\delta^2)$.

Let us first consider the region $z = O(1)$. Introducing (4.10) and $\kappa = 3/4 + \delta\mathsf{k}$ reduces (4.1) to

$$\hat{u}'' + \frac{\bar{\phi}'}{\bar{\phi}}\hat{u}' + \left[\frac{1}{\delta^2} \frac{9z(z-3)}{16(1+z)} + \frac{1}{\delta} \left(\frac{9z}{16} \frac{2(z^2-1) - (1-z)^2}{(1+z)^2} + \frac{3\mathsf{k}z(z-3)}{2(1+z)} \right) \right] \hat{u} = O(1).$$

Seeking a solution in the WKB form

$$\hat{u} = \mathcal{A}(y) \left(a\mathrm{e}^{\Phi/\delta} + b\mathrm{e}^{-\Phi/\delta} \right), \quad \text{with} \quad \Phi = \Phi_0 + \delta\Phi_1 + O(\delta^2), \qquad (A\,12)$$

leads to

$$\Phi_0(z) = \frac{3}{4} \int_z^1 \left[\frac{3-z'}{z'(1+z')} \right]^{1/2} dz', \qquad (A\,13)$$

$$\Phi_1(z) = \mathsf{k} \int_z^1 \left[\frac{3-z'}{z'(1+z')} \right]^{1/2} dz' + \frac{3}{8} \int_z^1 \frac{2(1-z'^2) + (1-z')^2}{z'^{1/2}(1+z')^{3/2}(3-z')^{1/2}} dz'. \quad (A\,14)$$

The behaviour for $\delta^2 \ll z \ll 1$, required for matching, readily follows as

$$\Phi = \Phi_* - \frac{3\sqrt{3z}}{2} + O(z, \delta^2), \qquad (A\,15)$$

with

$$\Phi_* = \Phi_0(0) + \delta\Phi_1(0). \qquad (A\,16)$$

We next consider the region $z = O(\delta^2)$. Because

$$k^2 \left(\frac{\bar{c}^2}{\phi} - 1 \right) = O(1) \quad \text{for} \quad z = O(\delta^2),$$

the $O(1/k)$-accurate or, equivalently $O(\delta)$-accurate approximation (4.6) to σ must be used, and the $O(1)$ terms in (4.1) must be taken into account. Defining the $O(1)$ scaled variable ζ by

$$z = \delta^2 \zeta,$$

we approximate (4.1) as

$$\frac{d^2\hat{u}}{d\zeta^2} + \frac{1}{\zeta}\frac{d\hat{u}}{d\zeta} - \frac{27(\zeta - \zeta_*)}{16\zeta^2}\hat{u} = O(\delta), \quad \text{where} \quad \zeta_* = \frac{8}{9}\left(k - \frac{31}{24} \right). \tag{A 17}$$

Clearly, there is a turning point in the domain — and hence an instability — only if $k > 31/24$. This provides the estimate (4.17) for the cutoff wavenumber.

Equation (A 17) can be solved explicitly in terms of modified Bessel functions of imaginary order. In the notation of Dunster (1990), we write the general solution as

$$\hat{u} = \alpha K_{i\nu}(s) + \beta L_{i\nu}(s), \tag{A 18}$$

where α and β are arbitrary constants,

$$s = \frac{3\sqrt{3\zeta}}{2}, \quad \text{and} \quad \nu = \frac{3\sqrt{3\zeta_*}}{2} = (6k - 31/4)^{1/2}. \tag{A 19}$$

A relationship between α and β is obtained by imposing the radiation condition as $y \to \infty$, i.e. as $s \to 0$. Using the asymptotics

$$K_{i\nu}(s) \sim -\left(\frac{\pi}{\nu \sin(\pi\nu)} \right)^{1/2} \sin(\nu \log(s/2) - \varphi),$$

$$L_{i\nu}(s) \sim \left(\frac{\pi}{\nu \sin(\pi\nu)} \right)^{1/2} \cos(\nu \log(s/2) - \varphi),$$

as $s \to 0$, with $\varphi = \arg[\Gamma(1 + i\nu)]$ (Dunster 1990), we obtain from (A 18) the large-y behaviour

$$\hat{u} \sim \left(\frac{\pi}{\nu \sin(\pi\nu)} \right)^{1/2} [\alpha \sin(\nu y/2 + C) + \beta \cos(\nu y/2 + C)],$$

where C is independent of y. The radiation condition for $y \to \infty$ then imposes

$$\frac{\alpha}{\beta} = i. \tag{A 20}$$

We now match (A 18) with (A 15). Using the asymptotics

$$K_{i\nu}(s) \sim \left(\frac{\pi}{2s} \right)^{1/2} e^{-s},$$

$$L_{i\nu}(s) \sim \frac{1}{\sinh(\pi\nu)} \left(\frac{\pi}{2s} \right)^{1/2} e^{s}$$

of the Bessel functions as $s \to \infty$ (Dunster 1990), we obtain from (A 12), (A 15), (A 18) and (A 20) that

$$\frac{ae^{\Phi_*/\delta}}{be^{-\Phi_*/\delta}} = \sinh(\pi\nu)\frac{\alpha}{\beta} = i\sinh(\pi\nu).$$

Applying the jump condition leads to an expression for c_1 similar to (A 7), from which

we deduce (4.18). Using (A 13)–(A 16), the exponent $2\Phi_*$ can be written explicitly as $2\Phi_* = b_1 + \delta b_2$, with

$$b_1 = \frac{3}{2} \int_0^1 \left[\frac{3-z}{z(1+z)} \right]^{1/2} \mathrm{d}z, \qquad (A\,21)$$

$$b_2 = 2\mathsf{k} \int_0^1 \left[\frac{3-z}{z(1+z)} \right]^{1/2} \mathrm{d}z + \frac{3}{2}. \qquad (A\,22)$$

With ν given in (A 19), this provides a closed form approximation to the instability growth rate near the long-wave cutoff.

REFERENCES

BENDER C. M. & ORSZAG S. A. 1978 *Advanced Mathematical Methods for Scientists and Engineers.* McGraw Hill.

BOSS, E., PALDOR, N. & THOMPSON, L. 1996 Stability of a potential vorticity front: from quasi-geostrophy to shallow water. *J. Fluid Mech.* **315**, 65–84.

DUNSTER T. M. 1990 Bessel functions of purely imaginary order, with application to second-order linear differential equations having a large parameter. *SIAM J. Math. Anal.* **21**, 995–1018.

FORD, R. 1993 Gravity wave generation by vortical flows in a rotating frame. Ph Thesis, University of Cambridge.

FORD, R. 1994 The instability of an axisymmetric vortex with monotonic potential vorticity in rotating shallow water. *J. Fluid Mech.* **280**, 303–334.

FORD, R., MCINTYRE, M. E. & NORTON, W. A. 2000 Balance and the slow quasimanifold: some explicit results. *J. Atmos. Sci.* **57**, 1236–1254.

GILL A. E. 1982 *Atmosphere-Ocean dynamics* Academic Press.

KNESSL, C. & KELLER, J. B. 1992 Stability of rotating shear flow in shallow water. *J. Fluid Mech.* **244**, 605–614.

LORENZ, E. N. & KRISHNAMURTHY, V. 1987 On the nonexistence of a slow manifold. *J. Atmos. Sci.* **44**, 2940–2950.

MCWILLIAMS, J.C., MOLEMAKER J.M. & YAVNEH I. 2001 From stirring to mixing of momentum: Cascades from balanced flows to dissipation in the oceanic interior. In *Aha Huliko'a Proceedings 2001*, U. of Hawaii, 59–66.

MCWILLIAMS, J.C., MOLEMAKER J.M. & YAVNEH I. 2004 Ageostrophic, anticyclonic instability of a barotropic boundary current. *Phys. Fluids* **16**, 3720–3725.

MOHEBALHOJEH, A. R. & DRITSCHEL, D. G. 2001 Hierarchies of balance conditions for the f-plane shallow water equations. *J. Atmos. Sci.* **58**, 2411–2426.

NYCANDER J., DRITSCHEL D. G. & SUTYRIN G. G. 1991 The dynamics of long frontal waves in the shallow-water equations. *Phys. Fluids A* , **5**, 1089–1091.

PALDOR, N. 1983 Linear stability and stable modes of geostrophic currents. *Geophys. Astrophys. Fluid Dyn.* **24**, 299–326.

PLOUGONVEN R., MURAKI D. J. & SNYDER C. 2005 A baroclinic instability that couples balanced motions and gravity waves. *J. Atmos. Sci.* **62**, 1545–1559.

RIPA, P. General stability conditions for zonal flows in a one-layer model on the beta-plane or the sphere. *J. Fluid Mech.* **126**, 463–489.

VANNESTE, J. & YAVNEH, I. 2004 Exponentially small inertia-gravity waves and the breakdown of quasigeostrophic balance. *J. Atmos. Sci.* **61**, 211–223.

VANNESTE, J. 2004 Inertia-gravity wave generation by balanced motion: revisiting the Lorenz-Krishnamurthy model. *J. Atmos. Sci.* **61**, 224–234.

VIÚDEZ, A. & DRITSCHEL, D. G. 2004 Optimal PV balance of geophysical flows. *J. Fluid Mech.* **521**, 343–352.

WARN, T. 1997 Nonlinear balance and quasi-geostrophic sets. *Atmos. Ocean* **35**, 135–145.

YAVNEH, I., MCWILLIAMS J.C., & MOLEMAKER M.J. 2001 Non-axisymmetric instability of centrifugally stable, stratified Taylor-Couette flow. *J. Fluid. Mech.* **448**, 1–21.